Applied Catalysis B: Environmental 160–161 (2014) 400–407

Contents lists available at ScienceDirect

Applied Catalysis B: Environmental

journal homepage: www.elsevier.com/locate/apcatb

One-step reduction and functionalization protocol to synthesize polydopamine wrapping Ag/graphene hybrid for efficient oxidation of hydroquinone to benzoquinone

Weichun Ye[a,b,*], Xuezhao Shi[b], Jie Su[b], Yang Chen[b], Jiajia Fu[b], Xiaojuan Zhao[b], Feng Zhou[c], Chunming Wang[b], Desheng Xue[a,*]

[a] Key Laboratory for Magnetism and Magnetic Materials of MOE and Department of Physics, Lanzhou University, Lanzhou 730000, China
[b] State Key Laboratory of Applied Organic Chemistry and Department of Chemistry, Lanzhou University, Lanzhou 730000, China
[c] State Key Laboratory of Solid Lubrication, Lanzhou Institute of Chemical Physics, Chinese Academy of Sciences, Lanzhou 730000, China

ARTICLE INFO

Article history:
Received 18 December 2013
Received in revised form 4 May 2014
Accepted 22 May 2014
Available online 2 June 2014

Keywords:
Polydopamine
Reduced graphene oxide
Silver nanoparticles
Simultaneous reduction
Oxidation of hydroquinone

ABSTRACT

Based on the excellent properties of dopamine (reduction, self-polymerization and adhesion), we designed a one-step and environment-friendly reduction route to synthesize and simultaneously functionalize polydopamine (PDA)–Ag–reduced graphene oxide (RGO) hybrid. The obtained PDA–Ag–RGO hybrid was characterized by transmission electron microscopy, Raman spectroscopy, X-ray photoelectron spectroscopy, FT-IR and UV–vis analysis. Silver nanoparticles were uniformly dispersed on the surface of RGO sheets and coated with a thin PDA film. The hybrid exhibited good dispersivity in polar solvents (water and acetonitrile). Compared with Ag–RGO hybrid prepared via $NaBH_4$ reduction and commercial Pd/C catalyst, PDA–Ag–RGO hybrid had better catalytic activity for the oxidation of hydroquinone to benzoquinone in the presence of H_2O_2. Moreover, the hybrid still retained superior catalytic activity over multiple cycles.

1. Introduction

The catalyzed oxidation of hydroquinone to benzoquinone is an economic and ecological route to achieve the conversion of phenolic waste from industrial effluent to useful products. The latter compound (benzoquinone) and its derivatives have biologically important properties such as cardiovascular, antitumour, antibacterial, antigerminative and antiprotozoan activities [1–3]. Also, benzoquinones become an important class of industrial chemicals and are useful dienophiles in chemical transformations [4]. In the past decades, the homogeneously catalytic oxidation of hydroquinone has been employed by using mineral acids, simple metal ions and their complexes as catalysts [5,6], but most of these suffer from drawbacks such as homogenous reaction conditions and the generation of toxic wastes. Thus, the replacement of homogeneous processes by enviormentally friendly ones, which would employ heterogeneous catalysts and clean oxidants like O_2 and H_2O_2 has become a widely accepted strategy in fine chemicals synthesis [7–17]. The catalysts include mesoporous titanium-silicate catalyst [7,8], copper salts [9,10], platinum catalyst [11], silver oxide [12] and silver [13]. Furthermore, the use of immobilized catalysts for selective oxidation in liquid phase represents a great synthetic improvement [14,15].

Recently, graphene-based composites as a new class of hybrid materials have a received considerable attention due to synergistic and novel properties via the combination of metal or metal oxide nanoparticles [16,17]. Fundamentally, the methods involve the reduction of the mixture of graphene oxide (GO) and metal precursors by using chemical reductants such as hydrazine and sodium borohydride ($NaBH_4$). However, high temperatures and highly toxic reductants are generally required; moreover, the graphene-based composites exhibit poor dispersibility and tend to form agglomerates due to van der Waals interactions and strong π–π stacking, which limits their further applications [18,19]. Therefore, an alternative method is indispensable that is more environmental friendly and can simultaneously impart new functionality to the composites through covalent or noncovalent strategies.

Generally, surfactant, polymer, and amphipathic aromatic molecules have been widely used as stabilizer to improve the dispersibility and stability of graphene [20–22]. Among the various modifiers, polydopamine (PDA) shows the distinct advantages. As

* Corresponding authors at: Lanzhou University, Department of Chemistry, Tianshui nalu No.222, Lanzhou, Gansu 730000, China. Tel.: +86 931 8912589.
E-mail addresses: yewch@lzu.edu.cn (W. Ye), xueds@lzu.edu.cn (D. Xue).

http://dx.doi.org/10.1016/j.apcatb.2014.05.042
0926-3373/

a multifunctional biopolymer, PDA has been found as a surface-adherent coating with abundant amine and hydroxyl groups on a wide range of substrates by self-polymerization of dopamine (DA) in a weakly alkaline solution [23–25]. More importantly, as an eco-friendly and effective reducing agent, DA has recently been used for the reduction of $AgNO_3$ [26,27], $HAuCl_4$ [28,29], H_2PtCl_6 [30,31], and GO [27–31] instead of hazardous reducing agents such as $N_2H_4{\cdot}H_2O$ or $NaBH_4$.

In this work, based on the fascinating properties of DA (reduction, self-polymerization, and adhesion), PDA–Ag–reduced graphene oxide (RGO) hybrid was fabricated via the protocol of one-step reduction and simultaneous functionalization. The hybrid exhibited good dispersivity in polar solvents (water and acetonitrile). The catalytic activity and stability for the oxidation of hydroquinone to benzoquinone with H_2O_2 were investigated in detail.

2. Experimental

2.1. Chemicals

GO (purchased from Jiansin Scientific and Trading Co., Ltd.) was produced by the arc-discharge method. 3-Hydroxytyramine hydrochloride was obtained from Acros Organics. Silver nitrate, hydroquinone, benzoquinone, $NaBH_4$, Pd/C (10 wt% Pd loading) acetonitrile were purchased and used without further purification. Acetonitrile was of chromatographically pure. All other regents were of analytical grade.

2.2. Characterization

High-resolution transmission electron microscopy and corresponding selected area electron diffraction (HRTEM/SAED) were preformed on a transmission electron microscope (TEM, Tecnai G2 F30, FEI, USA). Energy dispersion X-ray (EDX) spectrum was used to analyze the composition of the samples. The samples for TEM were prepared by placing a drop of the as-prepared solution on carbon-coated copper grids followed by drying. An X-ray diffraction analyzer (XRD, Rigaku D/max-2400, Cu *K*-Alpha radiation, $\lambda = 0.1541$ nm) was used.

The surface morphologies of the samples were characterized with field emission scanning electron microscopy (FE-SEM, JSM-6701F, JEOL Inc., Japan). The composition of the samples was determined by XPS (PHI-5702, Physical Electronics, USA; monochromated Al-*K*α irradiation, with the binding energy of C1s at 284.8 eV as reference).

The Raman scattering measurements were performed at room temperature on a Raman system with confocal microscopy (Renishaw Microscope, Lab RAMHR800; laser excitation at 532 nm). The UV–vis and FT-IR spectra were recorded using a Perkin-Elmer Lambda UV–vis 800 spectrophotometer and a FT-IR spectrophotometer (Nicolet Nexus 670, USA), respectively.

2.3. Synthesis of PDA–Ag–RGO

In a typical procedure for the synthesis of PDA–Ag–RGO (10 wt% Ag loading), 10 mL of GO dispersion (1 mg mL^{-1}) was mixed with 50 μL of ammonia solution (28 wt% in water) under magnetic stirring, then 1 mL $AgNO_3$ solution (10 mM) was added to the dispersion under stirring for 1 h. Subsequently, 20 mL of Tris-buffer (10 mM, pH 8.5) with 0.5 mg mL^{-1} DA was added into the mixture and kept stirring at 60 °C overnight. The products were collected by centrifugation, thoroughly rinsed with water, and dried at 60 °C under vacuum. For comparison, PDA–RGO was prepared without $AgNO_3$ present in the reacted system under the similar conditions. Ag–RGO (10 wt% Ag loading) was obtained through the simultaneous reduction of GO and silver ions without adding any surfactants or stabilizers by using the conventional reduce agent ($NaBH_4$) under the similar conditions.

2.4. Catalysis process

The as-prepared PDA–Ag–RGO catalyst (1.0 mg) and 30% aqueous hydrogen peroxide (20 μL) were added to a solution of hydroquinone (2.0 mg) in MeCN (1.00 mL). The resulting suspension was sonicated at room temperature for different time. For comparison, the above Ag–RGO, PDA–RGO, and commercial Pd/C catalysts (containing 10 wt% Pd) were also used for catalytic oxidation of hydroquinone to benzoquinone under the same procedure.

The catalytic oxidation reaction was monitored by HPLC. The chromatographic system consisted of Varian 210 high performance liquid chromatographic pump (CA, USA), 325 UV–vis detector and Varian Star Chromatographic workstation. Chromatographic conditions included C18 column (5 μm, 4.6 mm × 250 mm, Dima Technology) and gradient elution (*A*: 1% (v/v) acetic acid aqueous solution, *B*: MeCN; 0 min *A* = 75%, *B* = 25%; 25 min *A* = 50%, *B* = 50%; 30 min *A* = 0%, *B* = 100%; 32 min stop) with a flow-rate of 1.0 mL min^{-1} and detection wavelength was 280 nm. Both mobile phase and analysis solutions were filtered through a 0.22-μm nylon membrane filter. The target compounds were identified by the relative retention time and diode array detection.

3. Results and discussion

3.1. Characterization of PDA–Ag–RGO

3.1.1. Morphologic characterization

The overall synthesis procedure of PDA–Ag–RGO is shown in Fig. 1. Previously, the silver(I) ions in solution were attached to the sites of the overall oxygen functional groups (such as carboxyl, carbonyl, hydroxyl and epoxide) on the GO surface due to electrostatic interactions. The redox potential of Ag^+/Ag ($E^0 = 0.80$ V) is more positive than that of GO/RGO ($E^0 = 0.35$ V) [32]. Also, the oxygen functional groups provide preferential reactive sites for the nucleation and anchoring of metal nanoparticles [33]. Afterward, the addition of the reducing agent (DA) to the precursor solution promotes the subsequent reduction of silver (I) ions which enables the growth of Ag nanoparticles on the GO surface, followed by the reduction of GO to RGO. PDA–Ag–RGO hybrid was further formed via self-polymerization of DA to PDA.

Fig. 2 presents TEM (Fig. 2a and b) and SEM (Fig. 2d) images of PDA–Ag–RGO hybrid. The impressive feature is that small nanoparticles are uniform (the diameter of 10–50 nm) and distributed on the graphene surfaces, which can be further proved by HR-TEM. Herein, we could not observe the interplanar spacing of Ag particle lattice (Fig. 2c). This might be ascribed to the wrapping of silver naoparticles with PDA coating. Fig. 2d presents the corresponding SEM image of PDA–Ag–RGO. The wrinkled nature of graphene not only supported a large surface area for metal nanoparticles but also played an important role in preventing graphene sheets from aggregation. In this graph (Fig. 2d), silver particles were distributed on the surface-wrinkled graphene sheets, which are recognized as bright spots, in which the shape of the silver particles was almost spherical with the irregular size dispersion (the diameter ranging from 10 to 60 nm). Fig. 2e shows that the diffraction dots were resolved in the SAED images, implying that Ag nanoparticles are highly crystallined. EDX spectrum in Fig. 2f confirms that these nanocrystals on the graphene sheets were metallic silver. Besides Ag, the element of C, O and Cu were detected as well. The peak of C belongs to graphene and supporting film of copper mesh. The existence of oxygen signal is from the PDA film. The signal indexed to Cu

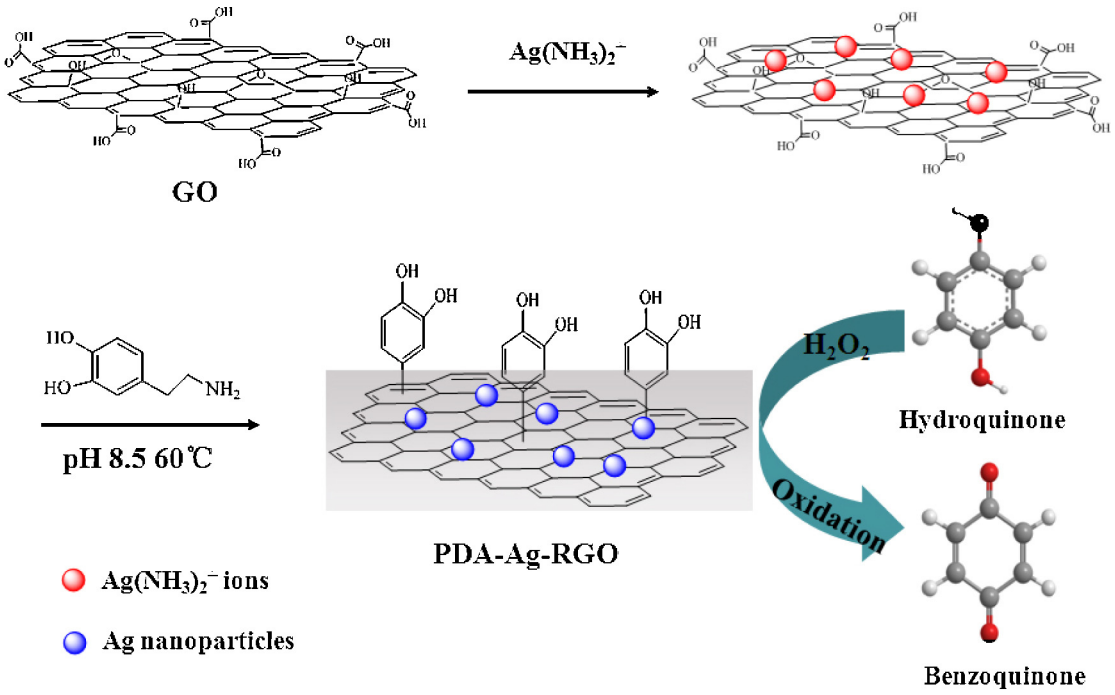

Fig. 1. The synthesis scheme of PDA–Ag–RGO hybrid for efficient oxidation of hydroquinone to benzoquinone.

is from a mesh used for the TEM measurement. The result of the EDX measurement suggests this method for synthesizing PDA–Ag–RGO hybrids is efficient and clean, without introducing any impurities.

For comparison, the morphologies of the Ag–RGO composites were observed by TEM (Fig. S1). It was found that the distribution of Ag nanoparticles on graphene surfaces was less homogeneous and some Ag nanoparticles were aggregated into large clusters. From the HR-TEM image (the inset of Fig. S1), the interplanar spacing of the Ag nanoparticles lattice is 0.23 nm, which is agreed well with the (1 1 1) lattice spacing of *fcc* Ag [34]. We believe that such a better distribution of silver nanoparticles for PDA–Ag–RGO is associated with the mild reducibility of DA.

3.1.2. Raman and XPS analysis

Raman spectroscopy is a useful and non-destructive tool to distinguish ordered and disordered carbon structures. As shown in Fig. 3, two characteristic peaks at 1353 and 1601 cm^{-1} were clearly observed, which are assigned to the D and G bands of graphene, corresponding to the symmetry A_{1g} mode and the E_{2g} mode of sp^2 carbon atoms, respectively. It was found that the D/G intensity ratio increased after reducing by DA and subsequently being coated with PDA. For PDA–RGO, the D/G intensity ratio was 0.96 while it decreased to 0.73 for pure GO. This change suggests a decrease in the size of the in-plane sp^2 domains and a partially ordered crystal structure of graphene. Furthermore, the G band of PDA–RGO shifted from 1610 to 1603 cm^{-1} in comparison to GO, which further confirms that GO was successfully reduced by DA. On the basis of the similarity in the Raman spectra of between PDA–Ag–RGO and PDA–RGO, it could be concluded that the decoration of Ag particles did not reduce the sizes of in-plane sp^2 domains of graphene [35]. Furthermore, XPS was performed to illustrate the composition of GO, PDA–RGO and PDA–Ag–RGO. The C1s XPS spectra of GO (Fig. 4a) indicates the presence of three main types of carbon bonds: C—C (284.8 eV), C—O (286.8 eV), and C=O (288.3 eV) [36]. For PDA–RGO (Fig. 4b) and PDA–Ag–RGO (Fig. 4c), the intensities of all C1s peaks of the carbon binding to oxygen decreased dramatically, which reveals that most oxygen containing functional groups were removed via the chemical reduction. Furthermore, an additional component at about 292 eV is attributed to a π–π^* "shake-up" satellite [37] of the aromatic rings of PDA. Although the wrapping mode of PDA is unclear [30], π–π stacking might be one of the possible interaction modes for PDA–RGO composites.

3.1.3. FT-IR and UV–vis spectra

The FT-IR was introduced to further characterize the functionalization of the hybrids. As shown in Fig. 5A, GO had the typical band at 1725 cm^{-1} due to the C=O stretching, suggesting the existence of oxygen functionalities at the GO surface [38]; in the FT-IR spectrum of PDA–RGO, the band at 2894 cm^{-1} of CH_n stretching vibration appeared while the band at 1725 cm^{-1} due to the C=O stretching disappeared. These suggest that GO has been successfully reduced to RGO and the graphene surface is wrapped with PDA via self-polymerization. Furthermore, it is found that the FT-IR spectrum of PDA–Ag–RGO was similar to that of PDA–RGO, which indirectly proves the coating of silver nanoparticles with PDA.

The simultaneous reduction process of GO and silver ions by DA was monitored by UV–vis absorption spectroscopy. As shown in Fig. 5B, two characteristic peaks appeared at 232 nm and 305 nm for GO nanosheets, which were due to $\pi \rightarrow \pi^*$ and $n \rightarrow \pi^*$ transitions, respectively. As GO was reduced to RGO, the $n \rightarrow \pi^*$ peak disappeared, while the absorbance peak at 232 nm shifted to 268 nm. Similar observation was obtained in the UV–vis spectra of PDA–Ag–RGO composites. Also, a weak band appeared at 400 nm in the absorption spectrum of GO–Ag sample, which was attributed to a surface Plasmon of silver nanoparticles [39]. Based on the above analysis from the FT-IR and UV–vis spectra, it could be concluded that GO and silver ions were simultaneously reduced, and the aromatic structure within the GO nanosheets restored during the reduction of DA.

3.2. Catalytic activity

The catalytic oxidation of hydroquinone using hydrogen peroxide as an oxidant over catalyst (Fig. 1) has become a main method for the large-scale production of benzoquinone, owing to its good

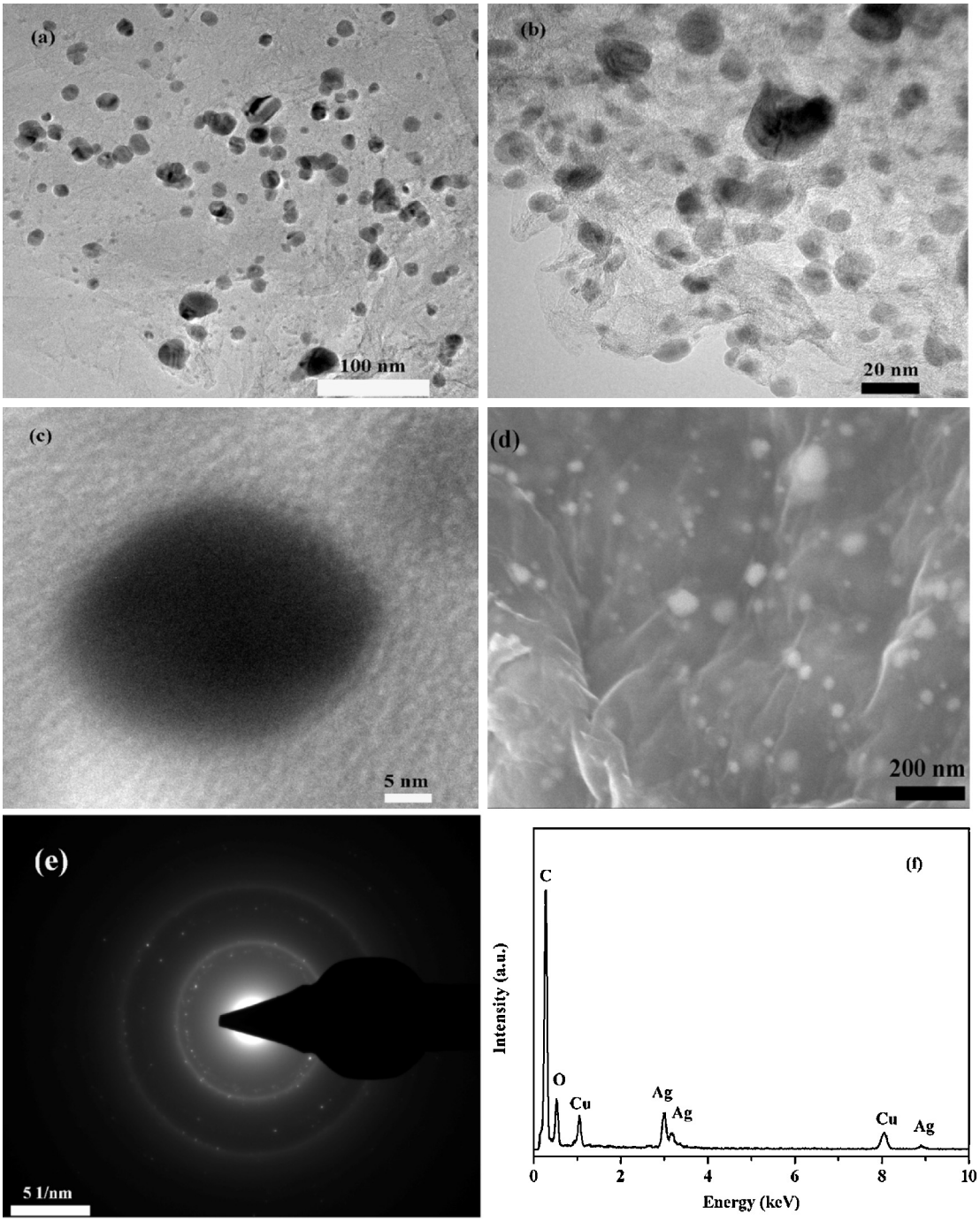

Fig. 2. PDA–Ag–RGO hybrid: TEM ((a) and (b)), HR-TEM (c) and SEM (d) images. (e) and (f) show the corresponding SAED and EDX patterns, respectively.

reputation of "green technology" [40–42]. Distinctly, the potential of the catalyst is directly concerned with the yield of the product. Herein, the catalytic activities of the functionalized Ag-graphene hybrids were tested in the oxidative reaction of hydroquinone to benzoquinone. The corresponding reaction equation is listed as follows:

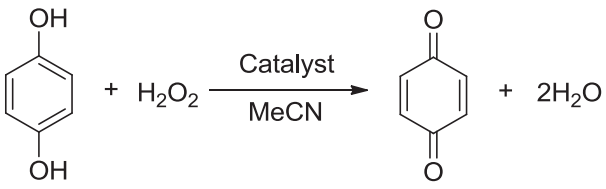

The reaction resultants are water except the product (benzoquinone). So, determining the amount of the raw material and product with HPLC analysis can effectively monitor the intensity of oxidation reaction. For hydroquinone, the retention time (t_r) kept at 10.8 min, while the t_r value was at 15.5 min for benzoquinone (Fig. S2).

We firstly evaluated the catalytic activity of the blank experiment, i.e., using PDA–RGO (without Ag nanoparticles) as the catalyst. Only 2% of conversion of hydroquinone after 1 h was given; even after 4 h, the percentage of conversion was only 11% (Fig. 6a and Fig. S3A). By contrast, as the PDA–Ag–RGO hybrids were added, a remarkable increase in conversion was observed. Through 1 h oxidation reaction, the conversion efficiency reached up to 87%. After

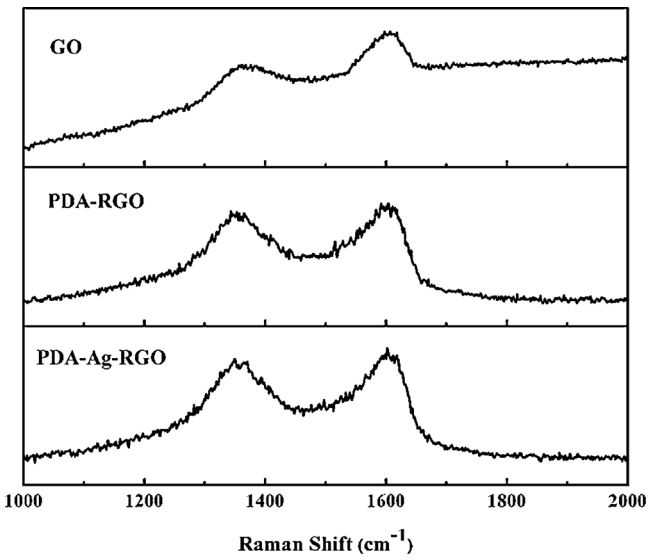

Fig. 3. Raman spectra of GO, PDA–RGO and PDA–Ag–RGO.

4 h, we almost observed the disappearance of hydroquinone (99% of conversion) and the formation of the desired benzoquinone (see Fig. 6b and Fig. S3B).

More importantly, the catalytic oxidation was completely selective (>99%) due to the competitive oxidative homo-coupling of hydroquinone. No other substituted products were observed in HLPC profiles. Similarly, there were no other peaks except the solvent (MeCN) and the product of benzoquinone by using gas chromatography detection (Fig. S4). These suggest that the functionalized Ag-graphene hybrids became highly efficient for the selective oxidation of hydroquinone to benzoquinone.

For comparison, we further studied the catalytic efficiencies of Ag–RGO and commercial Pd/C catalysts under the same process. The resulted conversion efficiencies are shown in Fig. 6c and d and Fig. S3C and D. Obviously, PDA–Ag–RGO hybrids were more efficient in the conversion of hydroquinone to benzoquinone than Ag–RGO and commercial Pd/C catalysts. After 1 h, the conversion efficiencies were only 70% for Ag–RGO catalyst and 72% for commercial Pd/C catalyst. Even after 4 h, the conversion efficiencies of both were still less than 90%. Since silver is much less expensive than palladium, developing a silver catalyst with a higher catalytic ability will bring great economic benefits.

UV–vis spectra were also used to prove the compared results. After 4 h oxidation, the reaction products were collected by removing the catalysts with centrifugation. Then the UV–vis spectra were recorded for the reaction products with 15-fold dilution. In Fig. 7, there was a weak peak at 290 nm in the case for the reaction product using PDA–Ag–RGO catalyst, which was similar to the case of pure benzoquione in acetonitrile (containing 2 mg/mL). The pure benzoquione was commercially purchased and of analytical grade (the content of 99%). The result indicates the complete conversion for the system using PDA–Ag–RGO catalyst. Conversely, the peak at 290 nm was much higher for the cases using Ag–RGO and Pd/C catalysts, which suggests that some hydroquinone could not be converted to benzoquione even after 4 h.

The turnover number (TON) and turnover frequency (TOF) are two important indicators to access the catalytic activity [43]. TON was calculated by dividing the concentration of the raw material (mol of hydroquinone) with the amount of the loading metal nanoparticles (mol of metal nanoparticles). TOF was calculated by dividing TON with the reaction time (h). The TON and TOF values for

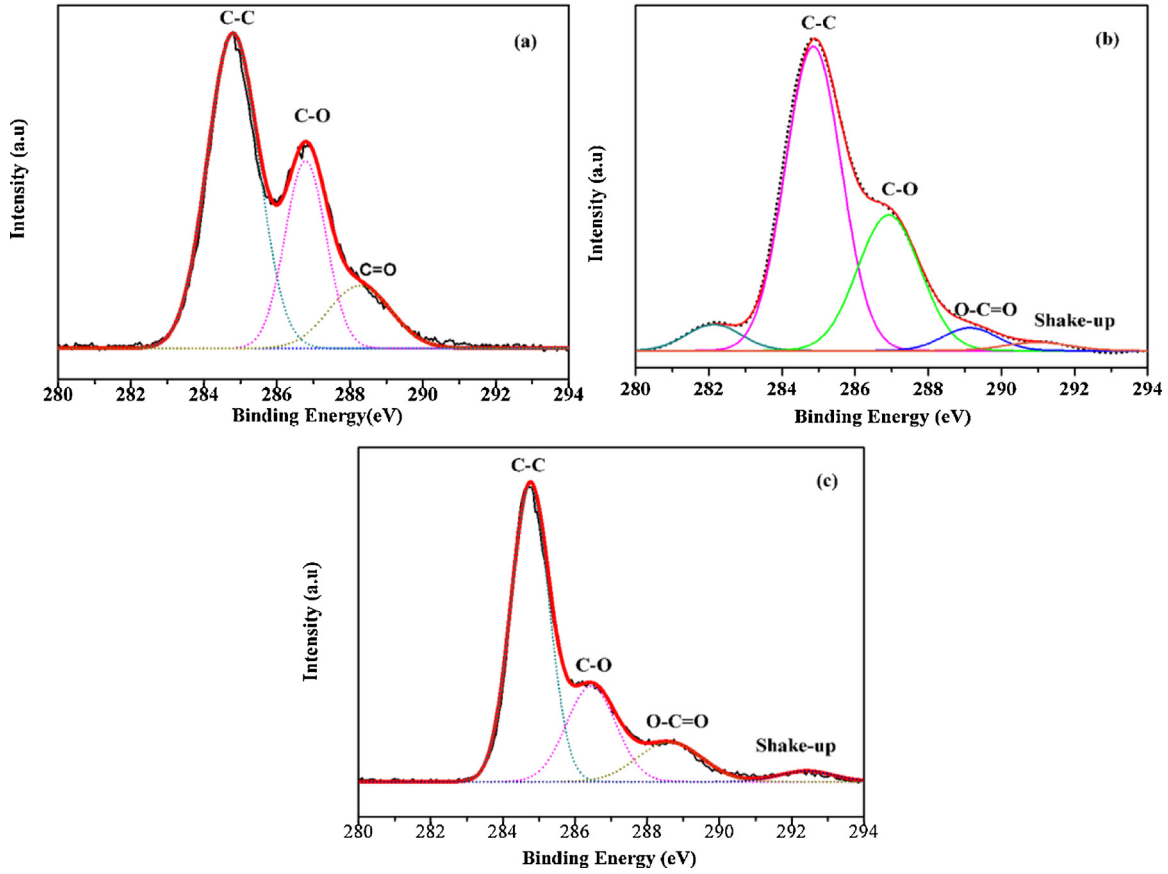

Fig. 4. XPS C1s core-level spectra of (a) GO, (b) PDA–RGO and (c) PDA–Ag–RGO.

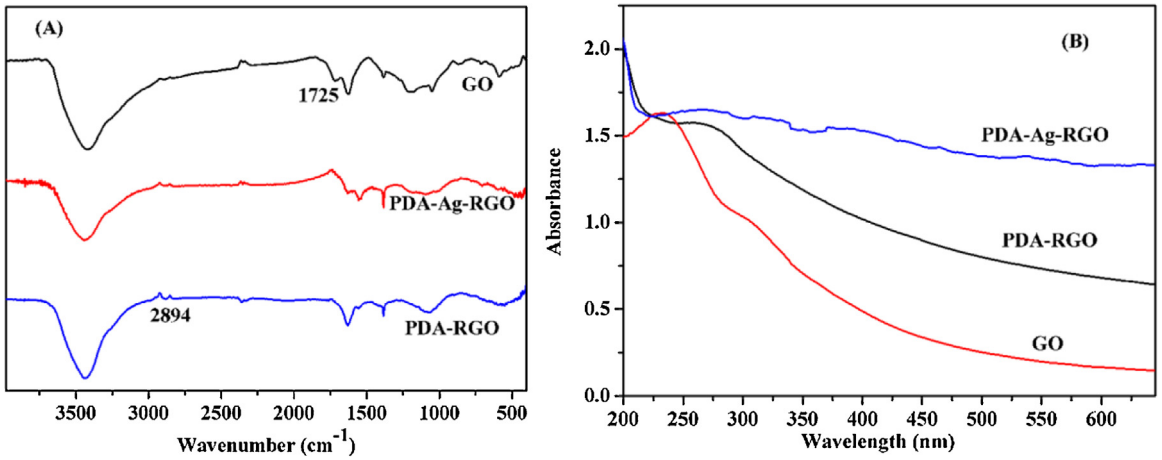

Fig. 5. FT-IR (A) and UV–vis (B) spectra GO, PDA–RGO and PDA–Ag–RGO.

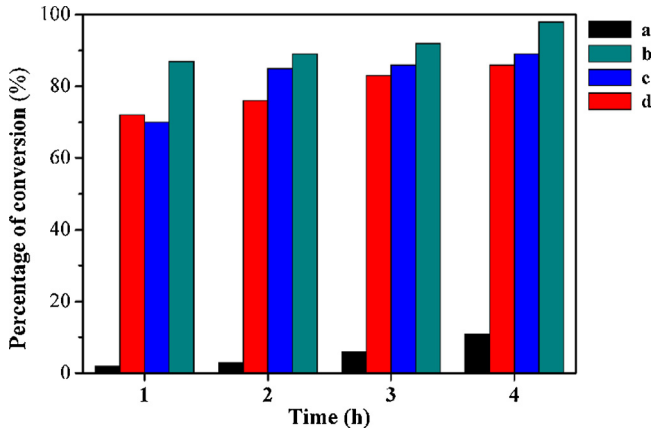

Fig. 6. Conversion efficiency of hydroquinone to benzoquinone for different catalysts. (a) Blank experiment (using PDA–RGO), (b) PDA–Ag–RGO, (c) Ag–RGO, (d) commercial Pd/C catalyst.

the three types of catalysts are listed in Table 1. The heterogeneous PDA–Ag–RGO hybrid feature the characteristics that are necessary for the reactions to occur at higher rate compared to Ag–RGO and commercial Pd/C catalysts. Metal complexes have been accepted

Table 1
Catalytic efficiency of the PDA–Ag–RGO hybrid in comparison to the reference systems.

Catalyst	Turnover number	Turnover frequency (h^{-1})
PDA–Ag–RGO	19.5	4.9
Ag–RGO	17.3	4.3
Commercial Pd/C	16.6	4.2

to efficiently catalyse this reaction [44,45]. However, it is found that the TON value of PDA–Ag–RGO hybrid is over 3 times of those of homogeneous and heterogeneous catalysts reported previously, where the homogeneous catalyst was cupper(II) complexes with a Schiff-base salen ligand [44] and the heterogeneous catalysts were this cupper(II) complexes encapsulated into NaY Zeolite [44] and cupper(II) complexes with aminoguanidyl and carboxyl groups immobilized on polymer support [45]. This suggests that PDA–Ag–RGO hybrid has considerably high catalytic activity in the oxidation of hydroquinone.

For heterogeneous catalysts, the dispersivity in reaction system is a key factor in enhancing the catalytic activity. Our results showed that PDA–Ag–RGO hybrid exhibited good dispersivity in polar solvent (water and acetonitrile) while a serious aggregation

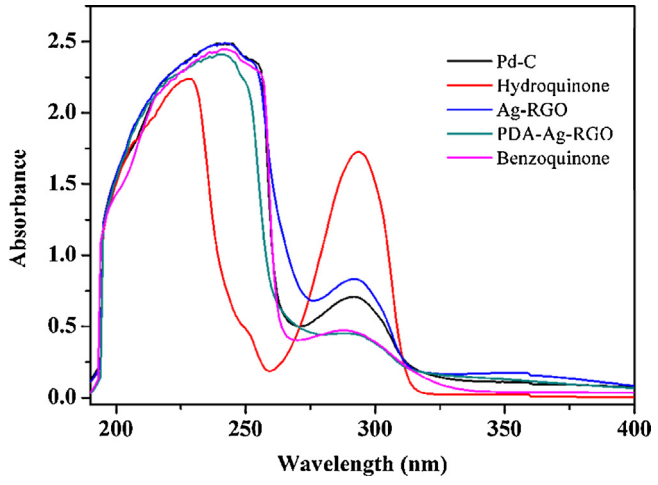

Fig. 7. UV–vis spectra of the cases with 15-fold dilution: pure hydroquione and benzoquione (respectively, both containing 2 mg/mL) in acetonitrile, the reaction products in the oxidation of hydroquione (2 mg/mL) using the catalysts of PDA–Ag–RGO, Ag–RGO, and Pd/C after 4 h.

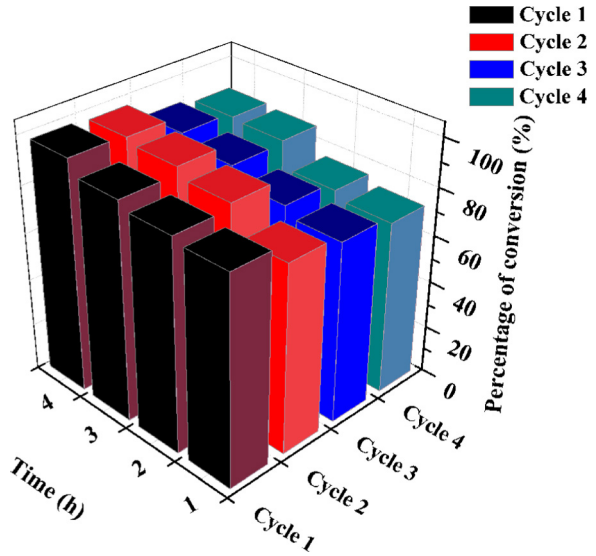

Fig. 8. Percentage of conversion following four cycles for catalytic reaction using PDA–Ag–RGO catalyst.

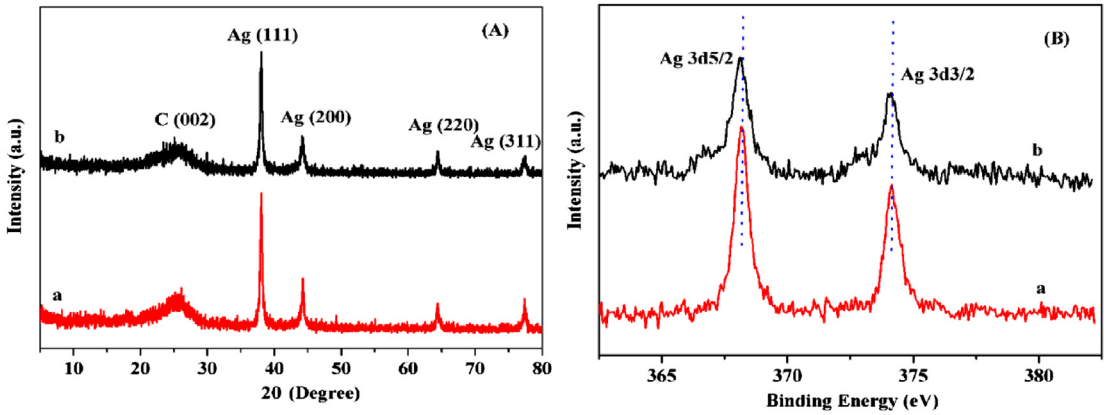

Fig. 9. The XRD (A) and XPS Ag 3*d* (B) patterns. (a) and (b) stand for the PDA–Ag–RGO catalyst before using for catalytic oxidation of hydroquione and after four cycles of re-using, respectively.

phenomenon occurred for Ag–RGO or commercial Pd/C catalysts (Fig. S5). Therefore, the good dispersivity of PDA–Ag–RGO hybrids resulted in a superior catalytic activity. Another positive factor is that PDA–Ag–RGO hybrid had smaller average size and the more uniform distribution of silver nanoparticles than Ag–RGO catalyst.

3.3. Catalytic stability

Considering the economic benefits, the recyclability of PDA–Ag–RGO catalyst was investigated by subjecting the catalyst systems to four cycles of re-using (Fig. 8). Under the same conditions, the second cycle gave similar excellent conversion. After more cycles of re-using, the conversion efficiency had a slight decrease (3rd and 4th cycle). Nonetheless, the percentages of conversion still exceeded 90%. These illustrated good stability of PDA–Ag–RGO catalyst. The XRD characterization of the recycled catalyst confirmed that the multi-cycle reaction did not obviously enlarge the size of Ag nanoparticles (Fig. 9A). From the XPS data, the valence state of Ag did not significantly change with the re-using of multiple cycles (Fig. 9B). That is probably because the coating of the functionalized PDA film prevented the silver nanoparticles from leakage and being washed away. This relative high stability could be attributed to no significant changes in the chemical composition and size of silver nanoparticles. Moreover, the hybrid is easily recovered by simple centrifugation and immediately recycled without any further purification. Therefore, it is promising for the benzoquinone production by selective oxidation of hydroquinone to the synthesis method of the functionalized PDA–Ag–RGO hybrid via the environment-friendly one-step reduction route.

4. Conclusions

We present a one-step reduction and functionalization protocol to synthesize PDA–Ag–RGO hybrid using the reduction, self-polymerization and adhesion properties of DA. The obtained PDA–Ag–RGO hybrid exhibited good dispersivity in polar solvents. It was shown that this hybrid exhibited superior catalytic activity and stability in the oxidation reaction of hydroquinone to benzoquinone. We believe that the one-step and environment-friendly method is expected for the controlled and effective design of new selective catalysts and for the production of advanced materials based on graphene with full exploitation of their properties.

Acknowledgements

This work is supported by the Natural Science Foundation of Gansu Province, China (No. 1107RJZA261), the Post-Doctoral Science Foundation of China (No. 2013M542393), the Fundamental Research Funds for the Central Universities (No. lzujbky-2012-25 and lzujbky-2012-26) and the Open Project of Key Laboratory for Magnetism and Magnetic Materials of the Ministry of Education, Lanzhou University (No. LZUMMM2014002).

Appendix A. Supplementary data

Supplementary data associated with this article can be found, in the online version, at http://dx.doi.org/10.1016/j.apcatb.2014.05.042.

References

[1] B.F. Sels, D.E. De Vos, P.A. Jacobs, Angew. Chem. Int. Ed. 44 (2005) 310–313.
[2] A. Gutenter, J.R. Ioset, E.F. Queiroz, C.M. Foggin, K. Hostettmann, Phytochemistry 58 (2001) 631–635.
[3] D.H. Miles, M. Payne, Tetrahedron 57 (2001) 5769–5772.
[4] B.H. Lipshutz, P. Mollard, S.S. Pfeiffer, W. Chrisman, J. Am. Chem. Soc. 124 (2002) 14282–14283.
[5] D. Mantzavinos, R. Hellenbrand, A.G. Livingston, I.S. Mecalfe, Appl. Catal., B: Environ. 7 (1996) 379–396.
[6] O. Cherkaoni, P. Nebois, H. Fillion, M. Domard, B. Fenet, Tetrahedron 52 (1996) 9499–9508.
[7] O.A. Kholdeeva, I.D. Ivanchikova, M. Guidotti, C. Pirovano, N. Ravasio, M.V. Barmatova, Y.A. Chesalov, Adv. Synth. Catal. 351 (2009) 1877–1889.
[8] D.G. Huang, X. Zhang, T.W. Liu, C. Huang, B.H. Chen, C.W. Luo, E. Ruckenstein, Z.S. Chao, Ind. Eng. Chem. Res. 52 (2013) 3762–3772.
[9] T. Sakamoto, H. Yonehara, C. Pac, J. Org. Chem. 62 (1997) 3194–3199.
[10] I. Owsik, B. Kolarz, J. Mol. Catal. A: Chem. 178 (2002) 63–71.
[11] H. Miyamura, M. Shiramizer, R. Matsubara, S. Kobayashi, Angew. Chem. Int. Ed. 47 (2008) 8093–8095.
[12] F. Derikvand, F. Bigi, R. Maggi, C.G. Piscopo, G. Sartori, J. Catal. 271 (2010) 99–103.
[13] P. Singh, G. Lamanna, C. Mnard-Moyon, F.M. Toma, E. Magnano, F. Bondino, M. Prato, S. Verma, A. Bianco, Angew. Chem. Int. Ed. 50 (2011) 9893–9897.
[14] C.M. Domínguez, P. Ocón, A. Quintanilla, J.A. Casas, J.J. Rodriguez, Appl. Catal., B: Environ. 144 (2014) 599–606.
[15] A. Quintanilla, S. García-Rodríguez, C.M. Domínguez, s. Blasco, J.A. Casas, J.J. Rodriguez, Appl. Catal., B: Environ. 111–112 (2012) 81–89.
[16] A.K. Geim, K.S. Novoselov, Nat. Mater. 6 (2007) 183–191.
[17] D. Chen, L. Tang, J. Li, Chem. Soc. Rev. 39 (2010) 3157–3180.
[18] S. Guo, S. Dong, E. Wang, ACS Nano 4 (2010) 547–555.
[19] S. Radhakrishnan, K. Krishnamoorthy, C. Sekar, J. Wilson, S.J. Kim, Appl. Catal., B: Environ. 148–149 (2014) 22–28.
[20] Y. Xu, H. Bai, G. Lu, C. Li, G. Shi, J. Am. Chem. Soc. 130 (2008) 5856–5857.
[21] J. Liu, J. Tang, J.J. Gooding, J. Mater. Chem. 22 (2012) 12435–12452.
[22] L. Li, X. Zheng, J. Wang, Q. Sun, Q. Xu, ACS Sustainable Chem. Eng. 1 (2013) 144–151.
[23] H. Lee, S.M. Dellatore, W.M. Miller, P.B. Messersmith, Science 318 (2007) 426–430.
[24] W. Ye, D. Wang, H. Zhang, F. Zhou, W. Liu, Electrochim. Acta 55 (2010) 2004–2009.
[25] W. Ye, H. Hu, H. Zhang, F. Zhou, W. Liu, Appl. Surf. Sci. 256 (2010) 6723–6728.
[26] J. Feng, P. Zhang, A. Wang, Q. Liao, J. Xi, J. Chen, New J. Chem. 36 (2012) 148–154.
[27] Z. Zhang, J. Zhang, B. Zhang, J. Tang, Nanoscale 5 (2013) 118–123.

[28] Y. Fu, P. Li, Q. Xie, X. Xu, L. Lei, C. Chen, C. Zhou, W. Deng, S. Yao, Adv. Funct. Mater. 19 (2009) 1784–1791.
[29] L. Guo, Q. Liu, G. Li, J. Shi, J. Liu, T. Wang, G. Jiang, Nanoscale 4 (2012) 5864–5867.
[30] L.Q. Xu, W.J. Yang, K.G. Neoh, E.T. Kang, G.D. Fu, Macromolecules 43 (2010) 8336–8339.
[31] Y. Li, Z. Wang, X. Liu, S. Yang, H. Wang, J. Ou, Z. Li, J. Wang, J. Mater. Chem. 22 (2012) 8036–8042.
[32] H. Yin, H. Tang, D. Wang, Y. Gao, Z. Tang, ACS Nano 6 (2012) 8288–8297.
[33] G. Goncalves, P.A.A.P. Marques, C.M. Granadeiro, H.I.S. Nogueira, M.K. Singh, J. Grácio, Chem. Mater. 21 (2009) 4796–4802.
[34] W. Ye, Y. Chen, F. Zhou, C. Wang, Y. Li, J. Mater. Chem. 22 (2012) 18327–18334.
[35] K.S. Subrahmanyam, A.K. Manna, S.K. Pati, C.N.R. Rao, Chem. Phys. Lett. 497 (2010) 70–75.
[36] J. Qiu, L. Shi, R. Liang, G. Wang, X. Xia, Chem. Eur. J. 18 (2012) 7950–7959.
[37] J. Zhang, H. Yang, G. Shen, P. Cheng, J. Zhang, S. Guo, Chem. Commun. 46 (2010) 1112–1114.
[38] C. Xu, X. Wang, Small 5 (2009) 2212–2217.
[39] J.M. Campos-Martin, G. Blanco-Brieva, J.L.C. Fierro, Angew. Chem. Int. Ed. 45 (2006) 6962–6984.
[40] W.R. Sanderson, Pure Appl. Chem. 72 (2000) 1289–1304.
[41] R. Maggi, C.G. Piscopo, G. Sartori, L. Storaro, E. Moretti, Appl. Catal., A: Gen. 411 (2012) 146–152.
[42] R.K.P. Purushothaman, J. van Haveren, D.S. van Es, I. Melin-Cabrera, J.D. Meeldijk, H.J. Heeres, Appl. Catal., B: Environ. 147 (2014) 92–100.
[43] I. Kuzniarska-Biernacka, M.A. Carvalho, S.B. Rasmussen, M.A. Bañares, K. Biernacki, A.L. Magalhães, A.G. Rolo, A.M. Fonseca, I.C. Neves, Eur. J. Inorg. Chem. 2013 (2013) 5408–5417.
[44] G.M.S. ElShafei, F.Z. Yehia, O.I.H. Dimitry, A.M. Badawi, G. Eshaq, Appl. Catal., B: Environ. 99 (2010) 242–247.
[45] I.A. Owsik, B.N. Kolarz, Catal. Today 91–92 (2004) 199–204.